

Proceedings of the Korean Nuclear Society Autumn Meeting
Yongpyong, Korea, 2003

A Computational Analysis for The Cold Crucible Melting of Corium

Jin Ho Song, Beong Tae Min, Seong Wan Hong
Korea Atomic Energy Research Institute
P. O. Box 105, Yuseong Post Office, Taejeon, 305-600, Korea

Soon Hyo Chung
Korea Institute of Science and Technology
39-1 Hawolgok-dong, Seongbuk-gu, Seoul, 136-791, Korea

Abstract

To investigate the performance of the cold crucible method employed for melting corium, which is a mixture of UO_2 and ZrO_2 , computational analyses of the coupled electro-magnetic field, heat transfer and fluid flow are performed. Governing differential equations, basic numerical methods, computational models, and the results are discussed. It is shown that the outstanding features of cold crucible melting observed in the experiments are well reflected in the computational analyses results.

1. Introduction

One of the techniques for the melting of refractory material is the cold crucible melting method [1,2], which is also called the skull melting method. The skull that is formed between the very high temperature melt and the cold crucible acts as a self-container and an effective insulator. The cold crucible melting is basically inductive heating of an electrically conducting melt by an alternating electromagnetic field. Heating is accomplished by Ohmic losses caused by eddy currents induced in the melt itself [3]. Recently, the technique is widely spread and used in the nuclear industry. To perform an experiment to simulate the molten fuel and coolant interaction phenomenon of severe accidents in a nuclear reactor [4], it was necessary to make molten liquid from a mixture of UO_2 and ZrO_2 , which are the major constituents of reactor material. However, as it has a very high melting temperature, the development of a melting technique for these materials accompanies difficult engineering problems. It was successfully applied to the fuel coolant interaction experiment using a mixture of UO_2 and ZrO_2 [5]. US DOE applied this technique for the immobilization of high-activity waste [2].

While significant demands exist in the nuclear industry, the implementation of cold crucible technique for certain application encounters many engineering problems and little

data is available for the characteristics of the cold crucible. Therefore, a computational tool, which can predict the performance of cold crucible melting reliably, will be very helpful in solving practical problems. In this paper a computational model for the cold crucible melting is suggested and results of the analysis are discussed and compared with the experimental data.

2. Governing Differential Equations

The melting by a cold crucible involves complicated processes. The volumetric heat source produced by the Ohmic loss by the induced current increases the temperature of the mixture. When the temperature increases above the melting temperature of the mixture, the solid changes to a liquid. As the charged material is a binary mixture, there exist a liquid, solid, and mush zone.

When some of the mixture becomes liquid, a fluid motion starts due to both the buoyancy force and electromagnetic force. So, the analysis of cold crucible melting involves the analysis of the electromagnetic field around the cold crucible components and charged material, which could be a mixture of liquid, solid, and mush, and the fluid flow and heat transfer analysis of the charged material. The electromagnetic field, fluid flow and heat transfer process is closely coupled. The electromagnetic force acts on the fluid and heat source as the melting comes from the induction.

2.1 Governing Differential Equations for the Electro-magnetic Field

The governing differential equations for the electromagnetic field are described below [4]

$$\text{Ampere's law} \quad \nabla \times \mathbf{H} = \mathbf{J}_o + \mathbf{J}_e + \partial \mathbf{D} / \partial t \quad (1)$$

$$\mathbf{J}_e = \sigma \mathbf{E} \quad (2)$$

$$\text{Faraday's law} \quad \nabla \times \mathbf{E} = - \partial \mathbf{B} / \partial t \quad (3)$$

Gauss's law on the electric flux density and magnetic flux density are described as below

$$\nabla \cdot \mathbf{D} = \rho_c \quad (4)$$

$$\nabla \cdot \mathbf{B} = 0 \quad (5)$$

$$\mathbf{B} = \mu_m \mathbf{H} \quad (6)$$

$$\mathbf{D} = \epsilon \mathbf{E} \quad (7)$$

The electromagnetic force and Joule heating by induced current is described as

$$\mathbf{F}_{em} = \mathbf{J}_e \times \mathbf{B} \quad (8)$$

$$Q_{em} = \mathbf{J}_e \cdot \mathbf{J}_e / \sigma \quad (9)$$

By defining a magnetic vector potential \mathbf{A} , which is defined as

$$\nabla \times \mathbf{A} = \mathbf{B} \quad (10)$$

from equation (3), it follows $\mathbf{E} = -\partial \mathbf{A} / \partial t$ (11)

Then the Ampere's law in equation (1) can be rewritten as

$$\nabla \times (1/\mu_m \nabla \times \mathbf{A}) = \mathbf{J}_o + \sigma \mathbf{E} + \varepsilon \partial \mathbf{E} / \partial t = \mathbf{J}_o - \sigma \partial \mathbf{A} / \partial t - \varepsilon \partial^2 \mathbf{A} / \partial t^2 \quad (12)$$

For an electric field with an angular frequency ω , the above equation can be written as

$$\nabla \times (1/\mu_m \nabla \times \mathbf{A}) + i\omega \sigma \mathbf{A} - \varepsilon \omega^2 \mathbf{A} = \mathbf{J}_o \quad (13)$$

2.2 Governing Differential Equations for the Fluid Flow and Heat Transfer

The governing equations consist of the continuity equation, momentum equation, and energy equation [5]. The continuity equation

$$\partial \rho / \partial t + \nabla \cdot (\rho \mathbf{u}) = 0 \quad (14)$$

The momentum equation for the incompressible turbulent flow is

$$\partial (\rho \mathbf{u}) / \partial t + \nabla \cdot (\rho \mathbf{u} \mathbf{u}) = \mathbf{F}_{em} + \mathbf{F}_b + \mathbf{F}_d - \nabla p + \nabla \cdot (\mu + \mu_t) \nabla \mathbf{u} \quad (15)$$

Buoyancy force and the drag force in the solid liquid mixture [6],

$$\mathbf{F}_b = -\rho \beta \mathbf{g} (T - T_o) \quad (16)$$

$$\mathbf{F}_d = -C(1-f_l)^2/f_l^3 (\mathbf{u} - \mathbf{u}_s) \quad (17)$$

where f_l is the element liquid fraction, C is a constant accounting for the mushy-region morphology. The energy equation is

$$\partial (\rho C_p T) / \partial t + \nabla \cdot (\rho C_p \mathbf{u} T) = \nabla \cdot k_T \nabla T + Q_{em} + L(df_s/dT) \partial T / \partial t \quad (18)$$

where C_p is the specific heat of the liquid, k_T is the thermal conductivity, L is the latent heat, f_s is the solid fraction in a cell. The turbulence is modeled by the k - ε model equations [5]

$$\mu_t = \rho C_\mu k^2 / \varepsilon \quad (19)$$

$$\partial (\rho k) / \partial t + \nabla \cdot (\rho \mathbf{u} k) = \nabla \cdot (\mu + \mu_t / \sigma_k) \nabla k + G - \rho \varepsilon + S_{k,drag} \quad (20)$$

$$\partial (\rho \varepsilon) / \partial t + \nabla \cdot (\rho \mathbf{u} \varepsilon) = \nabla \cdot (\mu + \mu_t / \sigma_\varepsilon) \nabla \varepsilon + \varepsilon / k (C_{1\varepsilon} G - C_{2\varepsilon} \rho \varepsilon) + S_{\varepsilon,drag} \quad (21)$$

$$G = \mu_t (\partial u_i / \partial u_j + \partial u_j / \partial u_i) \cdot (\partial u_i / \partial u_j + \partial u_j / \partial u_i) \quad (22)$$

where $C_\mu = 0.09$, $\sigma_k = 1.0$, $\sigma_\varepsilon = 1.30$, $C_{1\varepsilon} = 1.44$, $C_{2\varepsilon} = 1.92$

$$S_{k,drag}=10^6[(1-f_1^2)/f_1^3]k \quad (23)$$

$$S_{e,drag}=10^6[(1-f_1^2)/f_1^3]\varepsilon \quad (24)$$

3. Numerical Analysis Method

To analyze the electromagnetic field around a cold crucible, which is made of segmented and water-cooled copper tubes, several numerical models have been applied. The finite element method, which solves the full three-dimensional field, is one of the numerical techniques to solve the governing differential equations [7]. Following are the finite element formulations. By multiplying a trial function Φ on both sides of equation (13) and taking the volume integral over the control volume V

$$\int \Phi \cdot [\nabla \times (1/\mu_m \nabla \times \mathbf{A})] dV + \int \Phi \cdot [i\omega \sigma \mathbf{A} - \varepsilon \omega^2 \mathbf{A}] dV = \int \Phi \cdot \mathbf{J}_o dV \quad (25)$$

By using the vector identity $\mathbf{a} \cdot (\nabla \times \mathbf{b}) = \nabla \times \mathbf{a} \cdot \mathbf{b} - \nabla \cdot (\mathbf{a} \times \mathbf{b})$ (26)

The first term in equation (25) becomes

$$\int \Phi \cdot [\nabla \times (1/\mu_m \nabla \times \mathbf{A})] dV = \int (\nabla \times \Phi) \cdot (1/\mu_m \nabla \times \mathbf{A}) dV - \int \nabla \cdot [\Phi \times (1/\mu_m \nabla \times \mathbf{A})] dV \quad (27)$$

By using Gauss's divergence theorem and the vector identity

$$\int \nabla \cdot \boldsymbol{\psi} dV = \int \boldsymbol{\psi} \cdot \mathbf{n} dS \quad (28)$$

$$\mathbf{a} \cdot (\mathbf{b} \times \mathbf{c}) = \mathbf{c} \cdot (\mathbf{a} \times \mathbf{b}) = -\mathbf{b} \cdot (\mathbf{a} \times \mathbf{c}) \quad (29)$$

the second term in equation (27) becomes

$$\begin{aligned} \int \nabla \cdot [\Phi \times (1/\mu_m \nabla \times \mathbf{A})] dV &= \int \mathbf{n} \cdot [\Phi \times (1/\mu_m \nabla \times \mathbf{A})] dS \\ &= \int (1/\mu_m \nabla \times \mathbf{A}) \cdot (\mathbf{n} \times \Phi) dS = -\int \Phi \cdot [\mathbf{n} \times (1/\mu_m \nabla \times \mathbf{A})] dS \end{aligned} \quad (30)$$

If we take the magnetic vector potential \mathbf{A} as the trial function, and use the relation $\mathbf{H} = 1/\mu_m \nabla \times \mathbf{A}$, equation (30) becomes

$$\int \nabla \cdot [\mathbf{A} \times (1/\mu_m \nabla \times \mathbf{A})] dV = \int \mathbf{H} \cdot (\mathbf{n} \times \mathbf{A}) dS = -\int \mathbf{A} \cdot [\mathbf{n} \times \mathbf{H}] dS \quad (31)$$

At only electrically or magnetically conducting boundary, the Equation (31) vanishes, because $\mathbf{n} \times \mathbf{A} = 0$ or $\mathbf{n} \times \mathbf{H} = 0$. At infinite boundary, it also vanishes because $\mathbf{A} = 0$ and $\mathbf{H} = 0$. At boundary between finite elements, $\mathbf{n} \times \mathbf{A}$ is continuous, so that surface integral for finite elements in both side of boundary compensates each other. Then equation (25) becomes

$$\int (\nabla \times \mathbf{A}) \cdot (1/\mu_m \nabla \times \mathbf{A}) dV + \int \mathbf{A} \cdot [i\omega \sigma \mathbf{A} - \varepsilon \omega^2 \mathbf{A}] dV = \int \mathbf{A} \cdot \mathbf{J}_o dV \quad (32)$$

The magnetic potential within each element in the non-conducting region can be interpolated by using the edge value

$$A = \sum A_i N_i \quad (33)$$

where N_i is the shape function. The put in equation (33) into equation (32)

$$\sum A_i \left[\int \sum (\nabla \times \mathbf{N}_i) \cdot (1/\mu_m \nabla \times \mathbf{N}_j) A_j dV + \int (i\omega\sigma - \epsilon\omega^2) \mathbf{N}_i \cdot \mathbf{N}_j A_j dV \right] = \sum A_i \left[\int \mathbf{N}_i \cdot \mathbf{J}_o dV \right] \quad (33)$$

Then it becomes

$$\sum \left[\int (\nabla \times \mathbf{N}_i) \cdot (1/\mu_m \nabla \times \mathbf{N}_j) A_j dV + \sum \int (i\omega\sigma - \epsilon\omega^2) \mathbf{N}_i \cdot \mathbf{N}_j A_j dV \right] = \int \mathbf{N}_i \cdot \mathbf{J}_o dV \quad (34)$$

From equation (34), we obtain a matrix equation

$$\mathbf{K}_{ij}^1 = \int (\nabla \times \mathbf{N}_i) \cdot (1/\mu_m \nabla \times \mathbf{N}_j) A_j dV \quad (35)$$

$$\mathbf{K}_{ij}^2 = \int (i\omega\sigma - \epsilon\omega^2) \mathbf{N}_i \cdot \mathbf{N}_j A_j dV \quad (36)$$

$$\mathbf{B}_i = \int \mathbf{N}_i \cdot \mathbf{J}_o dV \quad (37)$$

$$\sum (\mathbf{K}_{ij}^1 + \mathbf{K}_{ij}^2) A_j = \mathbf{B}_i \quad (38)$$

From this equation we determine the magnetic vector potential in each element. Then we can determine the electromagnetic force and Joule heating as below

$$\mathbf{B} = \nabla \times \mathbf{A}, \quad \mathbf{E} = -i\omega\mathbf{A}, \quad \mathbf{F}_e = \mathbf{J}_e \times \sigma \mathbf{E}, \quad \mathbf{Q}_{em} = \mathbf{J}_e \cdot \mathbf{J}_e / \sigma$$

The governing differential equation for the fluid flow and heat transfer are analyzed by the finite volume method [5]. As the procedure is well established, it is not repeated in this paper.

4. Analysis of Cold Crucible Melting

The analysis for the cold crucible melting of corium was performed by a computer program, which was built from the numerical method discussed above. As the electromagnetic field and fluid flow and heat transfer are coupled, the calculations were carried out in two steps. At first, the power distribution among crucible, charge, and coil was calculated by the analysis of electro-magnetic field around the crucible and Joule heat generation in the charge was calculated. Based on the Joule heat generation, the heat transfer and fluid flow analysis was performed to get the melt temperature, velocity of convective motion, and heat losses around the cold crucible.

4.1 Charging pattern

The charging pattern for the cold crucible and material model are shown below. The total weight of the charged material is about 17 kg. The corium was a mixture of UO_2 and ZrO_2 at

78:28 weight percent. The Zr ring in the center crucible is put as an initiator, as if the charged material contains only oxides, the Joule heat cannot not be generated in the charge.

In the material model, yellow region is plug and bottom portion of the crucible. The green region is the finger region. The white region is the induction coil. The initiator is gray. . The red region represents the mixture of UO_2 pellet and ZrO_2 powder. The blue region represents the ZrO_2 power layer. The vent hole is assumed to be is at the center

The electro-magnetic properties of cold crucible and electro-magnetic and thermo-physical properties of corium were provided as input. Different data are used for each material.

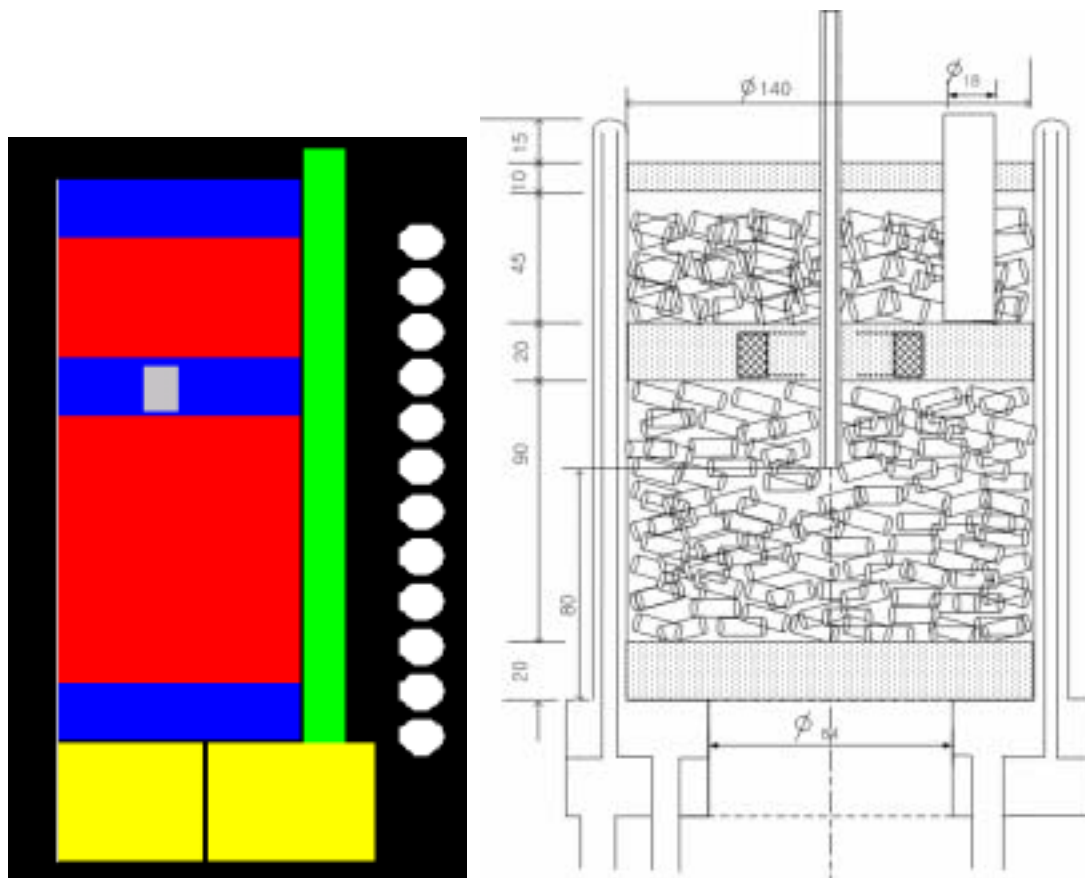


Figure 1 Actual charging pattern in the cold crucible and numerical model

4.2 Nodal scheme

As shown in the nodal scheme shown below, there are 25 nodes for the melt charge, 6 nodes for the finger, 6 nodes for the space between the finger and coil, 3 nodes for the coil, 6 nodes for the free space out side the crucible. There are 8 nodes in azimuthal direction in one segment as below. The one segment is defined for a single finger. The periodic boundary

conditions are applied. It is physically reasonable. As each segment will have the same initial and boundary condition.

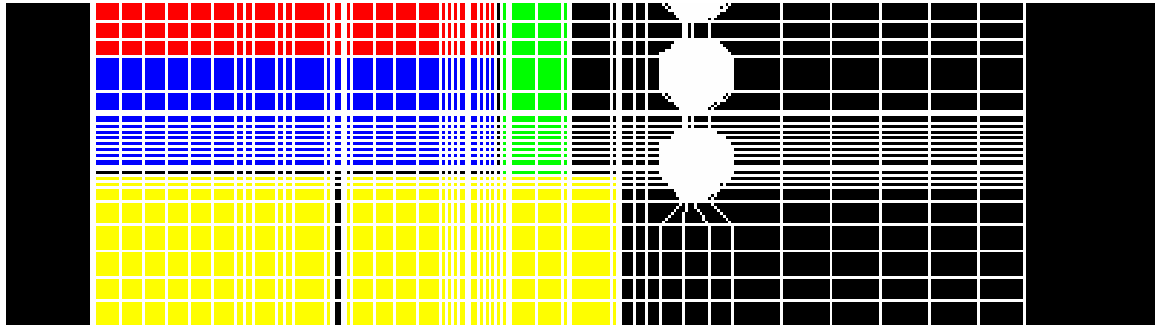


Figure 2 Node scheme for a part of vertical plane of cold crucible

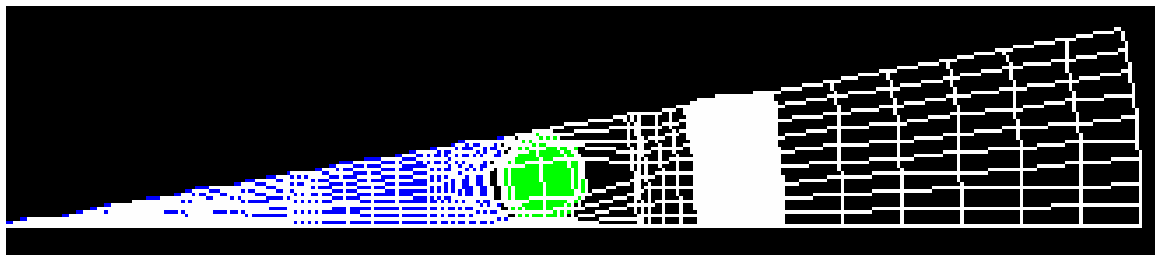


Figure 3 Node scheme in azimuthal direction for a segment of cold crucible

4.3 Analysis Results

The performance of cold crucible melting is analyzed by providing a constant power of 90 kW during the heating period, which is slightly higher than the average peak power in the real experiment. In the actual experiment, the power was slowly increased to minimize abrupt melt ejection. The melt ejection would destroy the upper crust and result in the direct contact with melt and crucible coil.

The results indicate that there are three distinct phases of initiation of melting by an initiator, initiation of close coupling between the melt and magnetic flux, and close coupling period. They were also found in the experiment. The results of analysis and discussions are provided for each phase.

4.3.1 Initiation of Melting

The input power to the cold crucible is assumed to be constant at 90kW. The flow pattern, isothermal lines at 300 seconds are shown in the Fig. 4(a), while the magnetic flux at this time is shown in Fig 4(a). The isothermal lines are at 200 °C interval and the yellow line

indicates 200 °C. The maximum temperature is 2344 °C. It is shown that the zirconium ring is almost melted and become a heat source for the nearby zirconia powder layer.

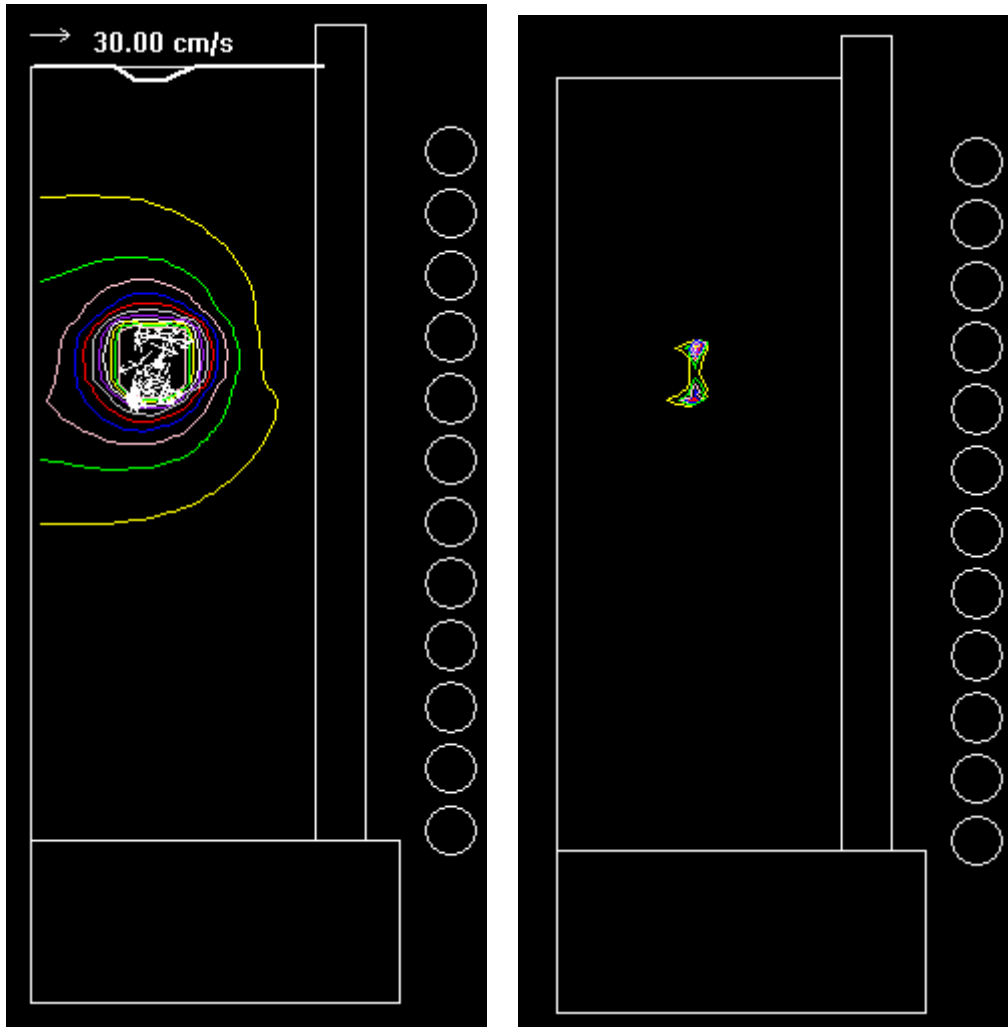


Figure 4 Fluid flow and isothermal lines(a)/ Joule heat Generation due to magnetic field(b)

The zone where Joule is generated is shown. The maximum flux is 1893 W/m^3 . Still the power consumption in the charge is very small compared to the total input power. The power consumed in the crucible and coil is 60.9 kW and 22.6 kW. They are dissipated as heat loss. The input power absorbed in the charge is 6.4 kW. So, the coupling between the charge and magnetic flux is weak.

4.3.2 Initiation of Close Coupling of Melt and Magnetic Flux

The left hand side figure indicates the fluid flow and isothermals at 1260 seconds. The isothermals are at 200 °C interval. The lowest isothermal line is yellow line near the bottom

portion of the crucible, which is 200 °C. The maximum temperature is 2643 oC. The power absorbed in the charge is 41.6 kW. The heat loss at the bottom, through the finger, and vent hole is 0.42 kW, 2.87 kW, and 0,015 kW. The remainder is used to heat up the charged material. The Joule heat generation is shown at the right hand side.

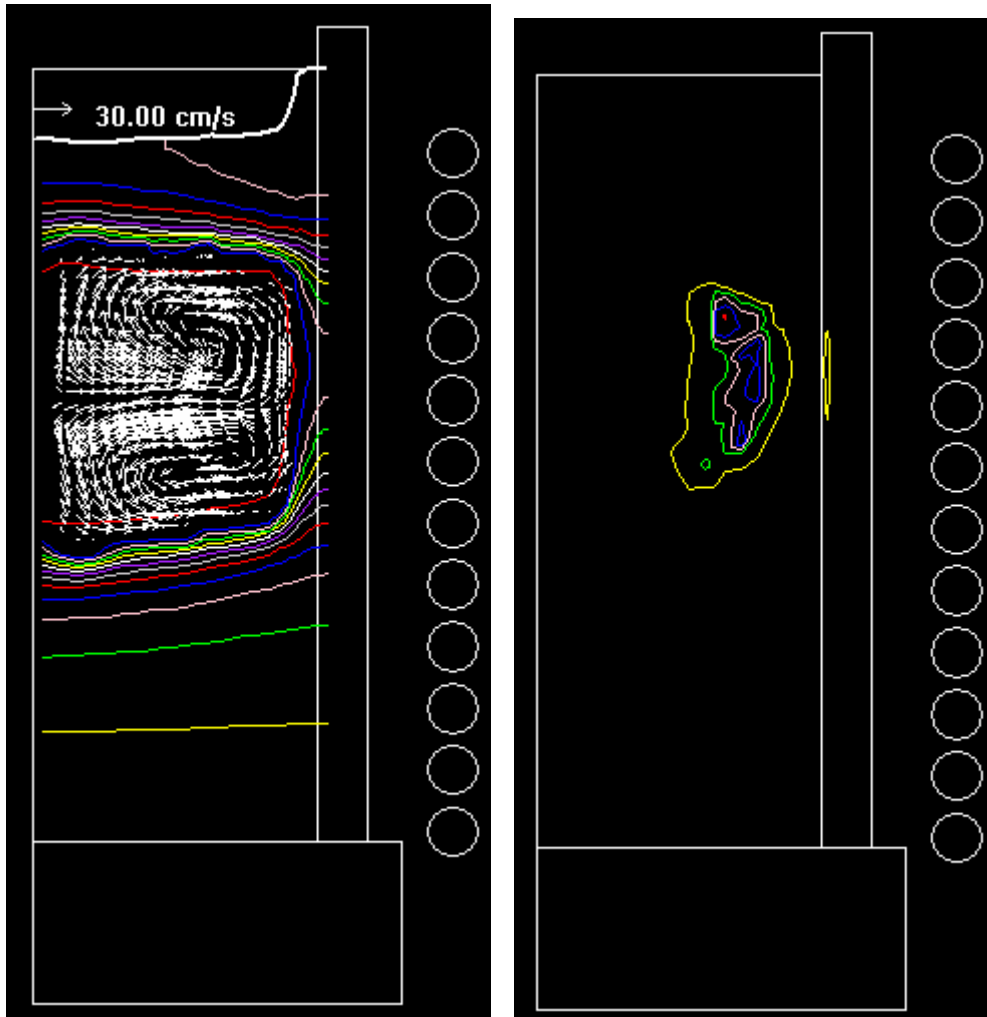


Figure 5 Fluid flow and isothermal lines(a)/ Joule heat Generation due to magnetic field(b)

4.3.3 Close coupling period

The power is supplied further to melt the charged material completely. The figures below indicate the fluid flow, isothermals, and joule heat generation at 2000 seconds. The isothermal lines are at every 100 °C starting from 2500 °C, which is yellow line. The maximum temperature is 3042 °C. It is shown the charged material is fully melted and there exist a thin layer at the bottom. There is a good mixing in the liquid region due to electromagnetic force and buoyancy force. The maximum speed is 33 cm/s. The flow is

turbulent regime. The absorbed power in the melt is 68.8 kW, while the heat loss to the finger, bottom, vent hole, and crust is 25.3 kW, 39.0 kW, 2.8 kW, and 8.2 kW. So, the balance is slightly negative. Then, the thickness of the lower crust would decrease a little bit to make the balance.

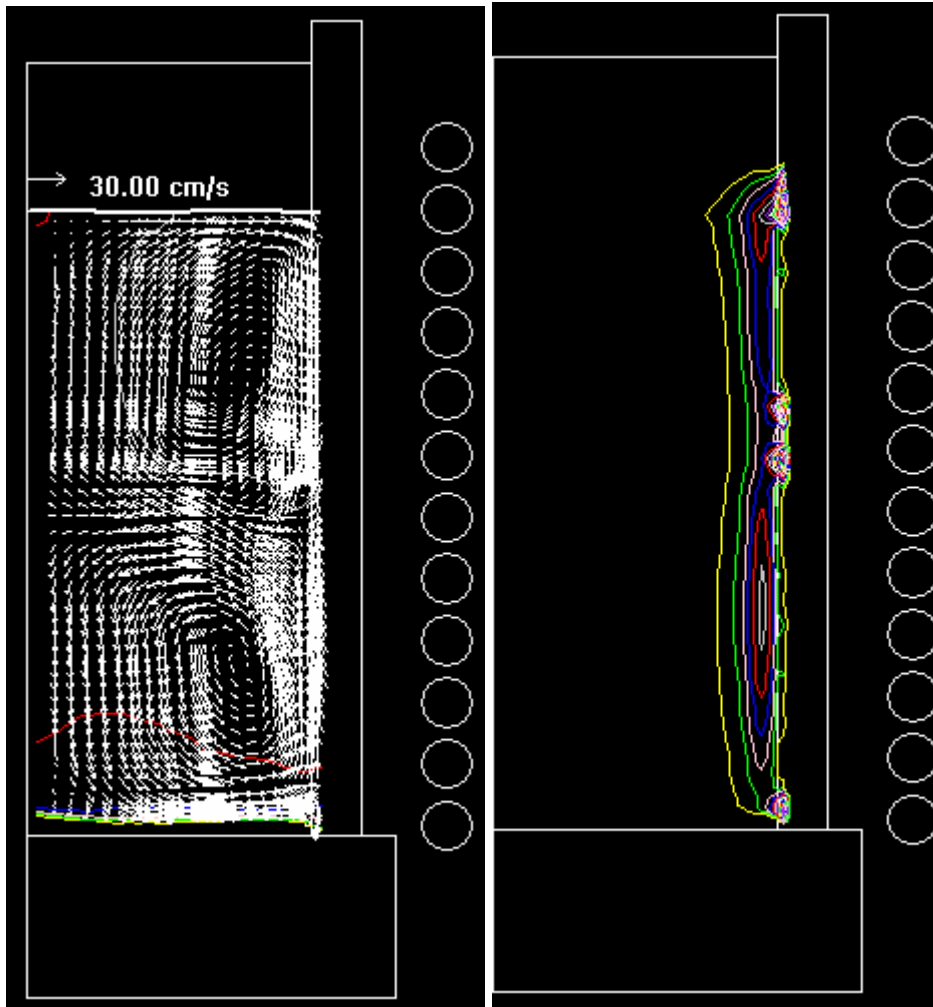


Figure 6 Fluid flow and isothermal lines(a)/ Joule heat Generation due to magnetic field(b)

The right hand side figure shows the joule heat generation. The lines indicate the contours of the same volumetric heat flux. The yellow line indicates 20.0 kW/cm³ and the lines are at every 20 W/cm³. It is shown that the heat generation is concentrated near the wall region, which is quite typical of induction heating of oxide material. At the lower part of the crucible, there is a plug region. After the charge is fully melted, the plug is removed and the puncher is automatically actuated to breach the bottom crust. The bottom crust should be thin enough to be fragile. So, after they are closely coupled, the power is used to heat up the

charged material at the lower part of the crucible. It is very necessary to minimize the unmelted lower layer for the melt delivery.

4.3.4 Power distribution in the cold crucible

Depending on the electromagnetic properties of charged material and cold crucible, the induction power is distributed. It changes as the melting progresses.

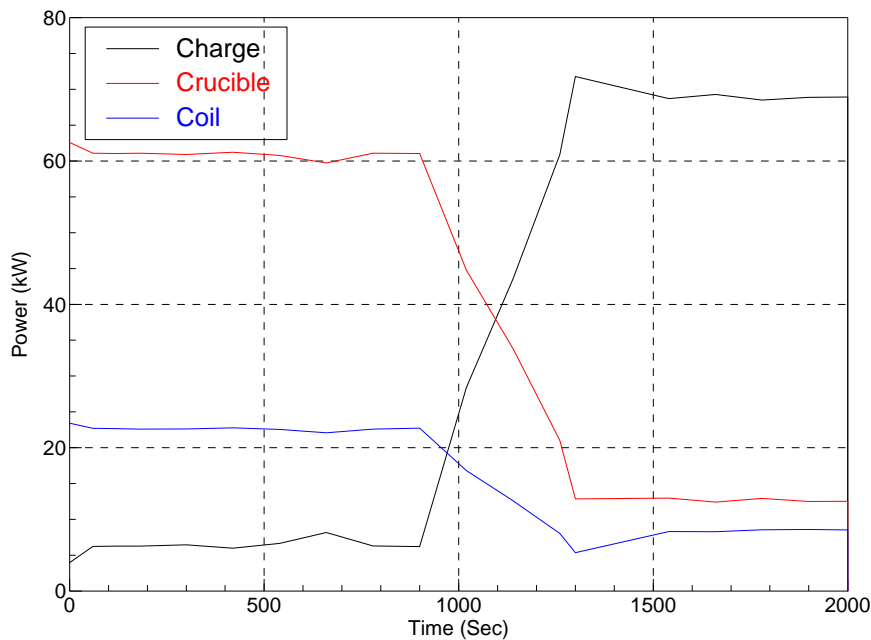


Figure 7 Power distributions in the crucible, charge and the induction coil

Initially the induction power is mainly dissipated to the crucible and induction coil, as there is only weak coupling between the magnetic flux and initiator. As the melting is progressed, the coupling increases. When, there is enough molten material, close coupling is initiated near 900 second as shown above. After that the induction heating is effective. The efficiency is 78 %.

4.3.5 Steady state balance, boundary conditions, and melt superheat

As the melt is maintained at a very high temperature, the heat loss occurs on the surface of the melt and through the vent hole on the top. Initially, the melting zone starts to form near the crucible wall and expands as the power is absorbed in the melt.

The solid-to-solid contact will accompany thermal boundary layer between the melt and the crucible, as there is a stiff temperature gradient. The heat loss through this wall increases as the absorbed power increases. When the input power is bigger than the heat loss, the remainder of the absorbed power is used to erode the crust layer. As the thickness of the crust layer decrease, the heat loss increases. So, a new steady state is reached. The heat loss through the vent hole is mainly by radiation, which is presented as

$$Q_{\text{vent}} = A\varepsilon v F v \sigma (T_m^4 - T_{\text{air}}^4)$$

and the energy loss by gas discharge.

There are two kinds of heat transfer between the melt and inner surface of the vertical wall of the crucible. The first one is the conduction heat transfer due to solid-to-solid contact. The second one is the radiation heat transfer considering the metal reflector, which can be represented as [11]

$$Q_{\text{rad}} = AF\sigma(T_1^4 - T_2^4)1/(1/\varepsilon_1 + 1/\varepsilon_2 - 1)$$

Here we considered explicitly the emissivity of corium and copper tube, which is 0.32 and 0.05 respectively. When we neglected the effect of copper tube wall, excessive heat loss through the crucible wall was observed. At the bottom of melt surface, solid-to-solid contact was assumed.

When the mixture is fully melted, the electromagnetic force pushes the molten liquid towards the center. So, there could be air gap between the vertical wall of the crucible and molten material, while solid-to-solid contact occurs between the bottom surface of the melt and the crucible. The melt super heat could be explained by assuming a air gap between the melt and the crucible in the vertical interface with the crucible. Then, the heat transfer is governed by the radiation transport.

5. Conclusion

A computational tool, which analyzes a coupled electromagnetic and thermal field around the cold crucible, for evaluation of the performance of a cold crucible melting is suggested. Though only qualitative comparisons are possible between the computational results and experimental results due to the limited measurements, the results of present analyses demonstrate that the fundamental characteristics of the cold crucible melting can be reliably predicted. It is suggested that the computational method proposed in the present paper can be effectively used for the design of a cold crucible and the analyses of cold crucible melting experiments.

Nomenclature

E : Electric field strength	H : Magnetic field strength
B : Magnetic flux density	J_o : Applied Electric current density
σ : Electric conductivity	ρ_c : electric charge density,
μ_m : Magnetic permeability	ϵ : Permittivity
ρ : Density	u : Velocity vector
μ : Viscosity	μ_t : Turbulent viscosity
F_{em} : Electromagnetic force	F_b : Buoyancy force,
F_d : Drag force in the solid liquid mixture	Φ : Trial function
A : Magnetic vector potential	N_i : Shape function

Acknowledgement

Present research was carried out under Mid and Long Term R&D supported by the Ministry Of Science and Technology of the Korean Government.

References

- (1) Kaldis, 1978, Current Topics in Material Science: Vol. 1, north- Holland, Chapter6: 421-480.
- (2) D. Gombert, J. R. Richardson, Cold-crucible induction melter design and development, Nuclear Technology, Vol. 141, No.3, 301-308, 2003
- (3) C. Gross, W. Assmus, A. Muiznieks, G. Raming, A. Muhlbauser, C. Stenzel, Power Consumption of Skull Melting, Part 1 Analytical aspects and experiments, Cryst. Res. Technol., 34, 3, 319-328.
- (4) J. H. Song, S. W. Hong, I. K. Park, B. T. Min, J. H. Kim, H. D. Kim, 2002, Spontaneous steam explosions observed in the fuel coolant interaction experiments using reactor materials, Journal of Korean Nuclear Society, Vol. 33(4), 344-357.
- (5) S. W. Hong, B. T. Min, J. H. Song, H. D. Kim, Application of Cold Crucible for Melting of UO₂/ZrO₂ Mixture, Materials Science and Engineering A357, 297-303, 2003.
- (6) W. H. Hayt, Jr., 1981, Engineering Electromagnetics, McGraw-Hill Book Company.
- (7) H. K. Versteeg and W. Malalasekera, 1995, An introduction to computational fluid dynamics, the finite volume method, Longman Group Ltd.
- (8). A. D. Brent, V. R. Voller, and K. J. Reid, 1988, Enthapy-porosity technique for the modeling convection-diffusion phase change: Appication to the meting of a pure metal, Numerical Heat Transfer, Vol. 13, 297-318.
- (9) Y. W. Cho, Y. J. Oh, K. W. Yi, S. H. Chung, and J. D. Shim, 1996, Numerical analysis of molten metal shape in cold crucibles by 3D FEM, Modelling Simul. Mater. Sci Eng. 4, 11-22.
- (10). Davies, E. J., 1990, Conduction and induction heating, Peregrinus, London.
- (11) 8. D. R. Gaskell, An Introduction to Transport Phenomena in Materials Engineering, 1992, Mcmillan Pub. Co., p.459.